Original Article

Assessment of ultrashort echo time (UTE) T_2* mapping at 3T for the whole knee: repeatability, the effects of fat suppression, and knee position

Zhenzhou Wu[1,2#], William Zaylor[1,2#^], Stefan Sommer[3,4], Dongxing Xie[1,2], Xiaodong Zhong[5], Kecheng Liu[6], Jeehun Kim[1,2], Jillian E. Beveridge[1], Xiaoliang Zhang[7], Xiaojuan Li[1,2,8]

[1]Program of Advanced Musculoskeletal Imaging (PAMI), Cleveland Clinic, Cleveland, OH, USA; [2]Department of Biomedical Engineering, Cleveland Clinic, Cleveland, OH, USA; [3]Advanced Clinical Imaging Technology (ACIT), Siemens Healthineers International AG, Zurich and Lausanne, Switzerland; [4]Swiss Center for Musculoskeletal Imaging (SCMI), Balgrist Campus, Zurich, Switzerland; [5]Siemens Medical Solutions USA, Inc., Los Angeles, CA, USA; [6]Siemens Medical Solutions USA, Inc., Malvern, PA, USA; [7]Department of Biomedical Engineering, University at Buffalo, State University of New York, Buffalo, NY, USA; [8]Department of Diagnostic Radiology, Cleveland Clinic, Cleveland, OH, USA

Contributions: (I) Conception and design: X Li; (II) Administrative support: X Li, JE Beveridge, K Liu; (III) Provision of study materials or patients: Z Wu, S Sommer; (IV) Collection and assembly of data: Z Wu, W Zaylor, D Xie, J Kim; (V) Data analysis and interpretation: Z Wu, W Zaylor, S Sommer, JE Beveridge, X Li; (VI) Manuscript writing: All authors; (VII) Final approval of manuscript: All authors.

[#]These authors contributed equally to this work as co-first authors.

Correspondence to: Xiaojuan Li, PhD. Department of Biomedical Engineering, Cleveland Clinic, Cleveland, OH, USA; Department of Diagnostic Radiology, Cleveland Clinic, Cleveland, OH, USA; Program of Advanced Musculoskeletal Imaging (PAMI), Cleveland Clinic, 9500 Euclid Ave, Cleveland, OH 44196, USA. Email: lix6@ccf.org.

Background: Knee tissues such as tendon, ligament and meniscus have short T_2* relaxation times and tend to show little to no signal in conventional magnetic resonance acquisitions. An ultrashort echo time (UTE) technique offers a unique tool to probe fast-decaying signals in these tissues. Clinically relevant factors should be evaluated to quantify the sensitivity needed to distinguish diseased from control tissues. Therefore, the objectives of this study were to (I) quantify the repeatability of UTE-T_2* relaxation time values, and (II) evaluate the effects of fat suppression and (III) knee positioning on UTE-T_2* relaxation time quantification.

Methods: A dual-echo, three-dimensional center-out radially sampling UTE and conventional gradient echo sequences were utilized to image gadolinium phantoms, one *ex-vivo* specimen, and five *in-vivo* subjects on a clinical 3T scanner. Scan-rescan images from the phantom and *in-vivo* experiments were used to evaluate the repeatability of T_2* relaxation time values. Fat suppressed and non-suppressed images were acquired for phantoms and the *ex-vivo* specimen to evaluate the effect of fat suppression on T_2* relaxation time quantifications. The effect of knee positioning was evaluated by imaging *in-vivo* subjects in extended and flexed positions within the knee coil and comparing T_2* relaxation times quantified from tissues in each position.

Results: Phantom and *in-vivo* measurements demonstrated repeatable T_2* mapping, where the percent difference between T_2* relaxation time quantified from scan-rescan images was less than 8% for the phantom and knee tissues. The coefficient of variation across fat suppressed and non-suppressed images was less than 5% for the phantoms and *ex-vivo* knee tissues, showing that fat suppression had a minimal effect on T_2* relaxation time quantification. Knee position introduced variability to T_2* quantification of the anterior cruciate ligament, posterior cruciate ligament, and patellar tendon, with percent differences exceeding 20%, but the meniscus showed a percent difference less than 10%.

^ ORCID: 0000-0002-2463-226X.

© Quantitative Imaging in Medicine and Surgery. All rights reserved.

Conclusions: The 3D radial UTE sequence presented in this study could potentially be used to detect clinically relevant changes in mean T_2* relaxation time, however, reproducibility of these values is impacted by knee position consistency between scans.

Keywords: Magnetic resonance imaging (MR imaging); ultrashort echo time (UTE); knee imaging; knee position; fat suppression

Submitted Feb 06, 2023. Accepted for publication Oct 07, 2023. Published online Nov 22, 2023.
doi: 10.21037/qims-23-459
View this article at: https://dx.doi.org/10.21037/qims-23-459

Introduction

Ligaments, tendons, and menisci are connective tissues in the knee which impact the symptoms and outcomes of knee disorders such as osteoarthritis (OA) (1-3). The menisci are vital for proper knee function and protection of the articular cartilage, and ligaments and tendons contribute to joint stability (4,5). Previous studies reported that elevated T_2*, T_2 and/or $T_{1\rho}$ relaxation times are often associated with meniscal damage/tears, anterior cruciate ligament (ACL) injury, and knee OA (6-10). Ligaments, tendons, and menisci have high concentrations of organized collagen fibers, a lower concentration of proteoglycan and less water (11) compared to other tissues, resulting in short T_2* relaxation times. Short T_2* relaxation times cause tissues to have little to no detectable signal with conventional magnetic resonance (MR) techniques, but imaging sequences with ultrashort echo times (UTE) have been used to quantify T_2* relaxation time in ligaments, tendons, and menisci (6,12-18). Therefore, UTE-type sequences are attractive candidates for detecting signal from tissues with short or ultrashort T_2* relaxation times (13). Quantitatively assessing tissues with ultrashort T_2* relaxation times offers the potential to identify imaging biomarkers that are associated with early knee OA (6).

Variation in UTE based T_2* relaxation time introduced by clinically relevant imaging parameters and patient-related conditions require evaluation to determine the reliability and sensitivity needed to distinguish diseased from control tissues. Previous work has evaluated the reproducibility of UTE-T_2* quantifications for articular cartilage (19), patellar tendon (PT) (20), and compared T_2* to UTE-T_2* relaxation times quantified in the meniscus (16). However, these studies have not evaluated the effect that some other clinically relevant parameters have on T_2* quantifications, such as fat suppression and patient positioning. Tissues with short T_2* relaxation times may be partially saturated by the fat suppression pulse, leading to a lower signal intensity at UTEs, and overestimation of the tissue's T_2* relaxation time (12,21). UTE scans can be performed with and without fat suppression, and an understanding of the effect that fat suppression has on T_2* relaxation time quantifications would help comparisons between studies in the literature. Patient-related conditions, such as the positioning of the knee with respect to the magnetic field, may also have an effect on T_2* quantifications. Strong dipolar interactions in collagen-rich tissues are subject to the magic angle effect, which can contribute to considerable overestimation of T_2* relaxation times (22-24).

The goals of this study were to evaluate (I) the repeatability of T_2* relaxation time measured by a UTE research application sequence, and evaluate (II) the effect of fat suppression and (III) knee position on T_2* relaxation time quantification. The repeatability of UTE based T_2* relaxation time mapping was evaluated against a conventional gradient echo (GRE) sequence using scan-rescan images from standard gadolinium (Gd) phantoms and *in vivo* subjects. Effects of fat suppression on quantitative results were evaluated in phantoms and an *ex-vivo* pig knee specimen. The effects of knee position were evaluated using UTE-T_2* and conventional GRE-T_2* knee tissue relaxation times using *in-vivo* imaging of human subjects.

Methods

Pulse sequence

We utilized a dual-echo, three-dimensional non-selective, radial center-out UTE research application sequence on a clinical 3T scanner throughout this study. The 3D radial UTE research application sequence consisted of a short non-selective rectangular radio frequency (RF) pulse followed by a 20 μs transmit/receive switch time and a 100% asymmetric (half spokes) FID acquisition starting

© Quantitative Imaging in Medicine and Surgery. All rights reserved.

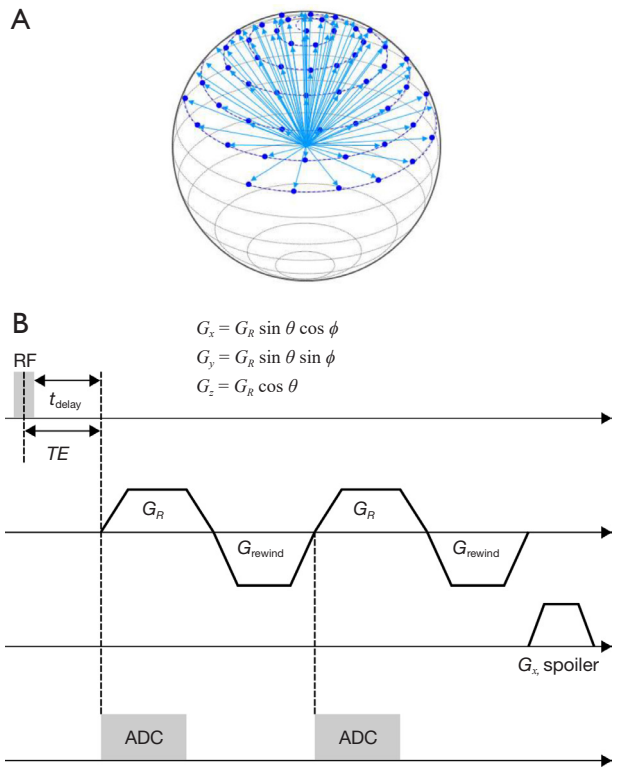

Figure 1 The sampling trajectory and sequence diagram for the 3D radial dual-echo UTE sequence. (A) A visualization of a 3D radial sampling trajectory; (B) the sequence diagram of the 3D radial dual-echo UTE sequence. RF, radio frequency; TE, echo time; ADC, analog to digital converter; 3D, three-dimensional; UTE, ultra-short echo time.

at the k-space center. To achieve an ultrashort TE, data acquisition started during ramp-up of the readout gradient. K-space was sampled using a 3D radial center-out trajectory with a koosh ball like distribution of spokes (*Figure 1*).

This 3D radial UTE prototype sequence can provide either single-echo or dual-echo acquisition. After the RF excitation pulse, the first echo was acquired from the k-space center to the surface of a sphere (inside-out readout) with UTE. A second echo can be acquired with either inside-out or outside-in trajectory corresponding to the polarity (monopolar or bipolar) of the second readout gradient. All dual-echo UTE scans were performed with monopolar readout; therefore, an additional rewinder gradient was used after the first read out gradient (*Figure 1*). Image reconstruction was based on a conventional non-uniform fast Fourier transform (NUFFT) by Cartesian gridding using a Kaiser-Bessel window function. To reduce trajectory deviations due to gradient non-linearity, axis-specific gradient delay correction was used to during reconstruction.

Phantom, ex-vivo and in-vivo image acquisition and processing

Phantom, *ex-vivo* and *in-vivo* experiments were carried out for this study. All data were acquired without pre-scan normalization, which is a correction method that impacts image intensity uniformity. Acquiring images without pre-scan normalization avoids variations in signal intensity scaling between acquisitions and facilitates interleaving of multiple acquisitions with different echo times (TE). Manual frequency, transmit adjustment, and 3D shimming were performed before each test with a manually selected shim volume. Scans were performed on a 3T scanner (MAGNETOM Prisma, Siemens Healthcare, Erlangen, Germany) which as has a maximum gradient amplitude of 80 mT/m, and a slew rate of 200 T/m/s. All phantom and *in-vivo* experiments used a knee coil (1Tx/15Rx, QED), and the *ex-vivo* experiments used a flexible coil (4Rx). Multi-echo data were aligned with increasing TEs and voxel-wise T_2* relaxation time was determined by using mono-exponential least square fitting.

Phantom experiment

Two Gd phantoms with 15 and 30 mM concentrations were prepared and three sequences were utilized: (I) single-echo UTE, (II) dual-echo UTE, and (III) multi-echo GRE (25,26) (*Table 1*). To ensure that single- and dual-echo UTE sequences yielded similar signal for common TEs, "signal ratio" maps were generated, which divided echo images from the single-echo sequence by the corresponding echo-image from the dual-echo sequence. The mean signal ratio was calculated across a representative slice approximately perpendicular to the phantom's length. Regions of interest (ROI) for each phantom were generated from a representative axial, sagittal, and coronal slice with an automatic regional grow algorithm that was initialized with a manually defined seed point within each slice. Mean and standard deviation (SD) of T_2* relaxation times within each ROI were calculated.

The phantoms were also used to evaluate the effect of fat suppression on UTE-T_2* relaxation time quantification. Dual-echo UTE acquisitions without fat suppression and with different number of radial spokes (5, 10, 15, and 20) per fat suppression pre-pulse were acquired in both Gd phantoms. All fat suppressed acquisitions used a spectrally

© Quantitative Imaging in Medicine and Surgery. All rights reserved.

Table 1 Sequence parameters of UTE and GRE imaging for Gd phantom, *ex-vivo* specimen and *in-vivo* patients

Study type	Sequence		
	Single-echo UTE/DESS	Dual-echo UTE	Multi-echo GRE
Gd phantom	Single-echo UTE		
Scan time (min:s)	8:17 (per echo time)	8:17 (per acquisition for two echoes)	13:39
FOV (mm^3)	130×130×130	130×130×130	130×130×128
Matrix size (freq × phase × slice)	240×240×240	240×240×240	256×256×128
Resolution (mm^2)	0.542×0.542	0.542×0.542	0.508×0.508
Slice thickness (mm)	0.542	0.542	1.000
TR (ms)	24.9	24.9	25
TE (ms)	0.06, 2, 4.92, 7.5, 8.62, 10, 19.5	0.06/7.5, 2/8.62, 4.92/10, 7.5/19.5	4.92, 8.61, 12.80, 20.00
Flip angle (degrees)	6	6	6
BW (Hz/pixel)	465	465	455
Radial views	20,000	20,000	–
Fat suppression	Off	Off/on (spokes: 5, 10, 15, and 20)	Off
Ex-vivo/*in-vivo*	DESS		
Scan time (min:s)	5:50	10:09 per acquisition × 2	9:13
FOV (mm^3)	140×140×112	160×160×160	160×160×120
Matrix size (freq × phase × slice)	384×384×120 (*ex-vivo*); 384×384×160 (*in-vivo*)	240×240×240	256×256×120
Resolution (mm^2)	0.365×0.365	0.667×0.667	0.625×0.625
Slice thickness (mm)	0.700	0.667	1.000
TR (ms)	17.55	12.9	29
TE (ms)	6.02	0.06/4.92, 2/8	2.48, 6.86, 11.24, 15.62, 20, 24.38
Flip angle (degrees)	25	6	12
BW (Hz/pixel)	185	465	500
Radial views	–	45,000	–
Fat suppression	On	*Ex-vivo*: off/on (spokes: 5, 10, 15, and 20); *in-vivo*: on, 20 spokes	On

Gd, gadolinium; UTE, ultra-short echo time; DESS, dual echo steady state; GRE, gradient echo; FOV, field of view; TR, repetition time; TE, echo time; BW, bandwidth.

selective fat saturation pulse.

Ex-vivo experiment

The *ex-vivo* experiment utilized one secondary use pig hind limb. The hind limb was disarticulated at the hip, leaving the knee joint capsule and surrounding soft tissue undisturbed, then stored at –20 ℃ until it was thawed and brought to room temperature over a 36-hour period prior to imaging. The *ex-vivo* sample remained unfixed throughout the experiment. The *ex-vivo* limb was used to evaluate the effects of fat suppression on UTE-T_2* relaxation time quantification. Similar to the phantom experiment, all acquisitions utilized a dual-echo UTE sequence without fat suppression and with different number of radial spokes (5, 10, 15, and 20) per fat suppression pre-pulse.

In addition to the UTE sequence, dual-echo steady

© Quantitative Imaging in Medicine and Surgery. All rights reserved.

Table 2 The echoes that were excluded from T_2* relaxation time fitting

Sequence	ACL	PCL	PT	MEN
UTE (ms)	None	None	8.00	None
GRE (ms)	None	24.38	15.62, 20.00, 24.38	20.00, 24.38

ACL, anterior cruciate ligament; PCL, posterior cruciate ligament; PT, patellar tendon; MEN, meniscus; UTE, ultra-short echo time; GRE, gradient echo.

state (DESS) and multi-echo GRE sequences (*Table 1*) were acquired. The DESS images were used to segment anatomical structures. Three adjacent representative sagittal slices near the mid-substance of the ACL, posterior cruciate ligament (PCL), PT and the medial and lateral meniscus (MEN) were manually segmented. The DESS image was rigidly registered to the first echo of the UTE and GRE images. The estimated registration parameters from the DESS to the first UTE echo were applied to the four tissue segmentations to align the corresponding ROI in the UTE and GRE images (27). Mean and SD UTE-T_2* and GRE-T_2* relaxation time within each ROI for both Gd phantoms and *ex-vivo* knee tissue were calculated for the UTE and GRE images, respectively.

In-vivo experiment

Five healthy volunteers (2 males and 3 females) took part in the *in-vivo* study. This study was conducted in accordance with the Declaration of Helsinki (as revised in 2013) and approved by the Institutional Review Board of the Cleveland Clinic, written informed consent was obtained from the participants prior to human subject experiments. Subjects did not have reported knee pain, a history of knee injury, or inflammatory disease. Each volunteer was imaged with their knee in an extended position then imaged again with their knee flexed within the knee coil to assess the effects of knee position on T_2* relaxation time. For each knee position, dual-echo UTE, multi-echo GRE, and DESS images were collected (*Table 1*).

To evaluate T_2* repeatability, subjects were rescanned using the UTE (n=4) and GRE (n=3) sequences. Rescan images were collected within the same session as the initial images but after subjects had exited and re-entered the scanner. For each knee position, all UTE and GRE image data were rigidly registered to the first echo of the GRE image (17). Representative slices of four tissues (PT, ACL, PCL, MEN) were manually segmented on the GRE images in both the extended and flexed knee position (8 segmentations total for each volunteer). For each tissue, three sagittal slices were segmented near the midsection of the ligaments and tendon, and the body of the MEN. To ensure consistent ROIs between scan and rescan images, the rescan image data were also rigidly registered to the first echo of the original scan's GRE image. Each tissue's segmentation was manually inspected in the rescanned images, and if the mask was misaligned, then new segmentations were generated using the registered rescan image. Mean and SD of the T_2* relaxation time was calculated in each ROI. To avoid fitting to echoes with low signal to noise ratio (SNR), the T_2* relaxation time for each tissue was recalculated with the longest echo excluded if the average mean T_2* value across subjects (either in extended or flexed positions) was less than half the longest echoes' TE (*Table 2*).

The knee position in extended and flexed positions was quantified using the DESS images. A semi-automated approach was utilized to define ROIs for the femur and tibia bones in the extended and flexed knee positions, and surfaces were generated from the segmentations. An automated approach used the bone surfaces to define the fixed femoral and tibial coordinate systems (28), and the coordinate systems were used to determine the joint kinematics for each position (29).

Statistical analysis

The phantom and *in-vivo* studies were used to evaluate the repeatability of the UTE-T_2* relaxation time. The percent difference between each initial and repeated scan for the phantom and *in-vivo* images was calculated to evaluate the repeatability of mean T_2* relaxation time for the UTE and GRE sequences (*Table 3*). The percent difference was calculated for each subject's ROI, then averaged across all subjects. Additionally, a Bland-Altman analysis was used to evaluate the scan-rescan repeatability of T_2* relaxation time, where the limits of agreement were determined using the SD of the scan-rescan difference from the 95% confidence intervals of the t-distribution. The percent difference and

© Quantitative Imaging in Medicine and Surgery. All rights reserved.

Table 3 An overview of the comparisons and statistical measures used for each study

Study	Comparison	Statistical measure
Phantom	Scan *vs.* rescan	% Diff, ICC, Bland-Altman
	UTE *vs.* GRE	ICC
	Fat suppression	CV, ICC
Ex vivo	Fat suppression	CV, ICC
In vivo	Scan *vs.* rescan	% Diff, ICC, RMSD, Bland-Altman
	UTE *vs.* GRE	% Diff
	Extension *vs.* flexion	% Diff, ICC, RMSD

% Diff, percent difference; ICC, intraclass correlation coefficient; CV, coefficient of variation; RMSD, root mean square deviation; UTE, ultra-short echo time; GRE, gradient echo.

intraclass correlation coefficient (ICC) between imaging sequences was calculated to evaluate the agreement between T_2* relaxation time measures. All of the percent differences were calculated as the absolute difference between two values divided by the mean of the two values, all multiplied by 100. ICC was calculated using R Statistical Software (V4.1.3; R Core Team) using the irr package [V0.84.1; Gamer *et al.* (30)] with a two-way random model and type of absolute agreement. An ICC value above 0.90 indicates excellent agreement while values below 0.50 indicates poor repeatability (31). Additionally, the root mean square deviation (RMSD) in mean T_2* relaxation times between initial and repeated scans across subjects (*Table 3*) was calculated.

The effect of fat suppression on T_2* relaxation time quantification was evaluated using the phantom and *ex-vivo* images. The amount of variation introduced by fat suppression was evaluated by calculating the coefficient of variation (CV) across all levels of fat suppression (number of radial spokes per fat saturation pulse) for each ROI in the phantom and *ex-vivo* images. The ICC across non-fat suppressed and all fat suppressed images was calculated to evaluate the agreement between mean T_2* relaxation times (*Table 3*).

The reproducibility of T_2* relaxation time quantification for the UTE and GRE sequences was evaluated using the *in vivo* images in the extended and flexed knee position. The percent difference in mean T_2* values between knee positions was calculated for each ROI and averaged across subjects. Additionally, the RMSD for mean T_2* relaxation times between extended and flexed knee positions across subjects was calculated (*Table 3*). The agreement between calculated T_2* relaxation times using data acquired in the extended and flexed position was also evaluated by calculating ICC for each sequence.

Results

Images of both Gd phantoms had homogeneous signal distribution with no observable artifacts (*Figure 2A*,*2B*). The minimum mean coefficient of determination (R^2) (±SD) of the monoexponential fit across both phantoms and across the single and dual echo UTE and GRE sequences was 0.98 (±0.06). Within the phantom's ROI, the mean signal ratio between the single- and dual-echo acquisitions showed values above 1.00, and increased as the TE increased (*Figure 2C*,*2D*). T_2* relaxation time maps calculated from the single and dual-echo UTE sequences showed similar variations, where the average SD across slices was 0.66 and 0.64 ms, respectively.

The average mean T_2* relaxation times across the imaged planes for the single-echo UTE, dual-echo UTE and the multi-echo GRE images was 11.85, 11.25, 11.31 ms for the 15 mM Gd phantom, and 5.76, 5.52, and 5.59 ms for the 30 mM Gd phantom, respectively (*Table 4*). All of the sequence's percent difference in mean T_2* relaxation time between scan-rescan images was less than 8%, and the Bland-Altman analysis showed a mean difference less than 0.25 ms (*Figure 3*). The inter-sequence percent difference values were less than 3.5%, and inter-sequence ICC showed excellent agreement between estimated T_2* relaxation times (*Table 4*).

The *ex-vivo* UTE images showed that the ACL and PT had rapidly decaying signals between 0.06 and 8.00 ms (*Figure 4*). The minimum mean R^2 value of the monoexponential fit across all of the *ex vivo* images was 0.98 and 0.93 for the UTE and GRE sequences, respectively. Mean UTE-T_2* relaxation time showed little variation between scans with fat suppression and scans with different numbers of radial spokes after fat suppression (*Table 5*). The CV between scans was less than 5% for both phantoms and knee tissues, however, the tissues showed the shortest and longest UTE-T_2* relaxation time in the scan without fat suppression and with 5 spokes after fat suppression, respectively (*Table 5*). The largest difference in mean UTE-T_2* relaxation time between scans with and without fat suppression was less than 1.5 ms. The mean UTE-T_2* relaxation times calculated from the *ex-vivo* images were

© Quantitative Imaging in Medicine and Surgery. All rights reserved.

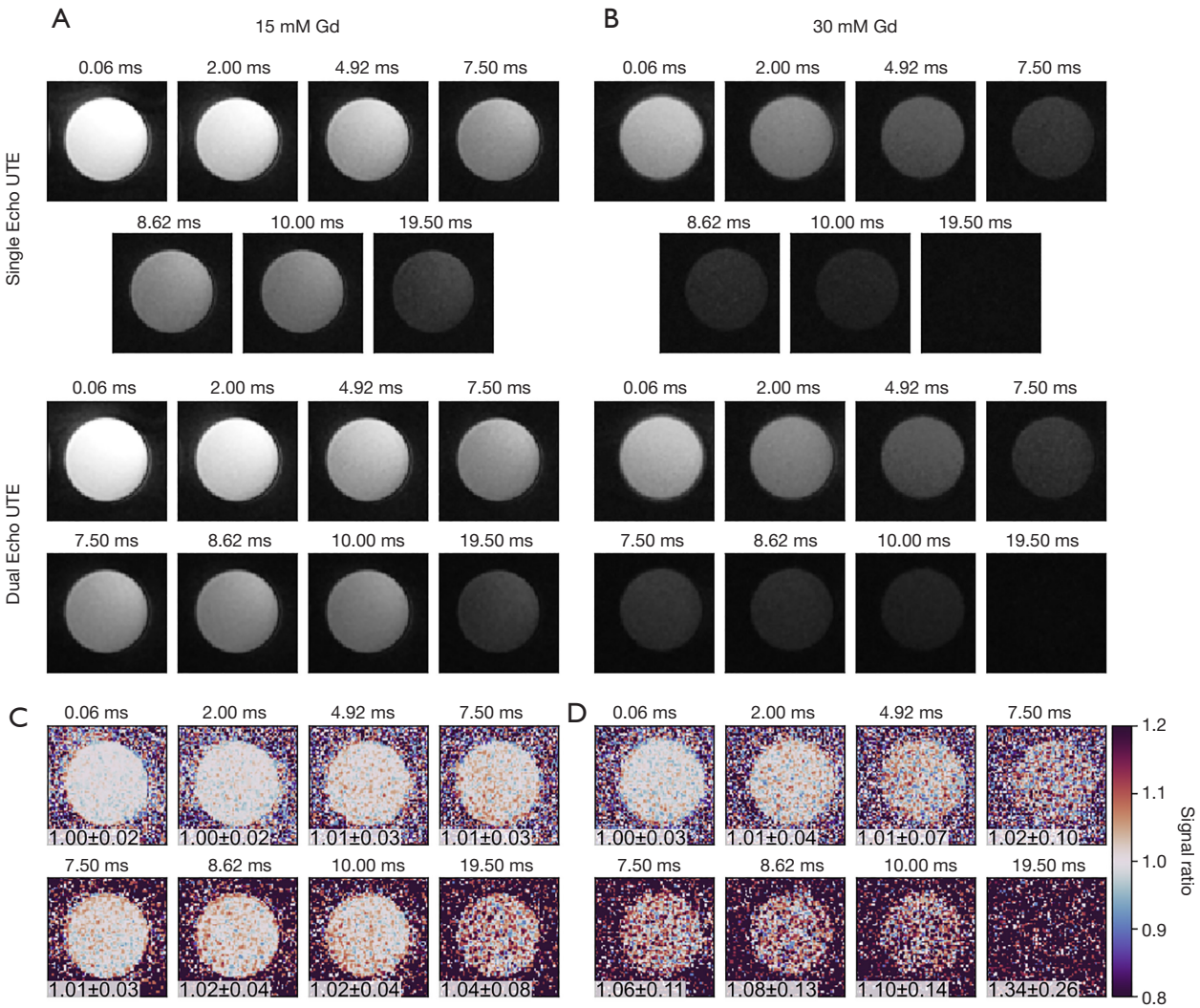

Figure 2 Signal intensity signal ratio maps from the phantom study. The single-echo and dual-echo UTE images of (A) 15 mM and (B) 30 mM Gd phantoms across the TEs. Corresponding signal ratio maps for (C) 15 mM and (D) 30 mM phantom between UTE echoes with same TE, where the inset shows the mean ± SD signal ratio within the ROI. UTE, ultra-short echo time; Gd, gadolinium; TE, echo time; SD, standard deviation; ROI, region of interest.

shorter than the GRE-T_2* relaxation times for each evaluated tissue, with the largest difference being nearly 8 ms (*Table 5*).

The *in-vivo* UTE images had shorter mean T_2* relaxation times compared to the corresponding tissues in the GRE images (*Figure 5*, *Table 6*). The average mean R^2 (±SD) of the monoexponential fit across subjects was greater than 0.95 (±0.02) for all tissues for both UTE and GRE sequences. For repeated scans, the UTE and GRE sequences had percent differences and RMSD less than 8% and 0.6 ms, respectively (*Table 7*). Similarly, the Bland-Altman analysis showed a mean difference in T_2* relaxation time between scan and rescan images less than 0.2 ms for both UTE and GRE sequences (*Figure 6*). Additionally, the UTE and GRE sequences had scan/rescan ICC values greater than 0.98 (*Table 7*).

The effect of knee position on the quantified T_2* relaxation times varied between tissues. Between the extended and flexed positions, subjects showed a mean ± SD change in flexion angle of 4.6°±3.2°. Overall, there was poor agreement between T_2* relaxation times determined from extended and flexed images, with ICC values of 0.51

© Quantitative Imaging in Medicine and Surgery. All rights reserved.

Table 4 The T_2* relaxation time of Gd phantoms using single-echo UTE, dual-echo UTE and multi-echo GRE without fat suppression, and the inter-sequence CV and ICC

Sequence	15 mM Gd phantom			30 mM Gd phantom		
	Axial	Coronal	Sagittal	Axial	Coronal	Sagittal
Single-echo UTE, ms						
First scan	11.88±0.58	11.98±0.90	11.67±1.41	5.83±0.13	5.78±0.33	5.69±0.53
Second scan	11.76±0.61	11.64±1.00	11.79±1.29	6.14±0.28	6.07±0.36	6.06±0.57
% Diff	1.04	2.88	0.96	5.21	4.98	6.44
Dual-echo UTE, ms						
First scan	11.32±0.47	11.37±0.69	11.06±1.34	5.59±0.12	5.53±0.33	5.44±0.52
Second scan	11.48±0.62	11.35±0.99	11.49±1.29	5.90±0.33	5.77±0.37	5.74±0.64
% Diff	1.38	0.20	3.81	5.33	4.33	5.34
Multi-echo GRE, ms						
First scan	11.35±1.20	11.33±1.31	11.23±1.52	5.65±0.52	5.58±0.65	5.55±0.76
Second scan	11.90±0.80	11.84±1.00	11.68±1.32	6.01±1.01	6.04±1.19	5.98±1.02
% Diff	4.79	4.35	3.96	6.27	7.97	7.46
Inter-sequence						
CV	2.75%	3.12%	2.82%	2.20%	2.35%	2.22%
ICC	0.993 (0.893–0.999)					

The inter-sequence CV and ICC values were calculating across the single-, dual-echo UTE, and the GRE T_2* values. Data are presented as the mean ± standard deviation, % Diff, CV and the ICC with 95% CIs. Gd, gadolinium; UTE, ultra-short echo time; GRE, gradient echo; CV, coefficient of variation; ICC, intraclass correlation coefficient; % Diff, percent difference; CI, confidence interval.

and 0.77 for the UTE and GRE sequences, respectively (*Table 6*). The UTE and GRE sequences showed the PT and ACL as having the highest RMSD in T_2* relaxation time between extended and flexed knee positions, respectively (*Table 7*). Both sequences showed the meniscus as having smallest change in T_2* relaxation times between knee positions, with RMSD and percent difference values less than 1.0 ms and 10%, respectively (*Table 7*).

Discussion

In this work, we presented and evaluated a 3D radial UTE prototype sequence to quantify T_2* relaxation time and tested its repeatability, the effect of fat suppression, and knee position for whole knee imaging against corresponding measures obtained from a more conventional GRE T_2* sequence. Previous studies have used other UTE sequences to evaluate the repeatability and reproducibility of UTE-T2* relaxation time quantified for knee imaging (19,20,32), and evaluated the effects of fat suppression on UTE-T_2* quantification (21,33). This current study utilizes a prototype sequence to quantify the variation in UTE-T_2* relaxation time introduced by clinically relevant factors such as knee positioning, and the quantified variations can be used to help identify the sensitivity needed to distinguish diseased from control tissues. In phantom scans with different Gd concentrations, low percent difference values indicate that both single-echo and dual-echo UTE sequences have excellent repeatability of T_2* relaxation times as well as high agreement with the conventional GRE sequence (25,26). The agreement in UTE-T_2* relaxation time between dual-echo UTE images acquired with and without fat suppression for the phantom and *ex-vivo* scans indicates that UTE-T_2* relaxation time is not sensitive to fat suppression. For *in vivo* human knees, both UTE and GRE T_2* relaxation time was repeatable, but showed variations between extended and flexed positions, indicating that orientation will have an effect on T_2* relaxation time quantifications.

The results from the phantoms show that quantification

© Quantitative Imaging in Medicine and Surgery. All rights reserved.

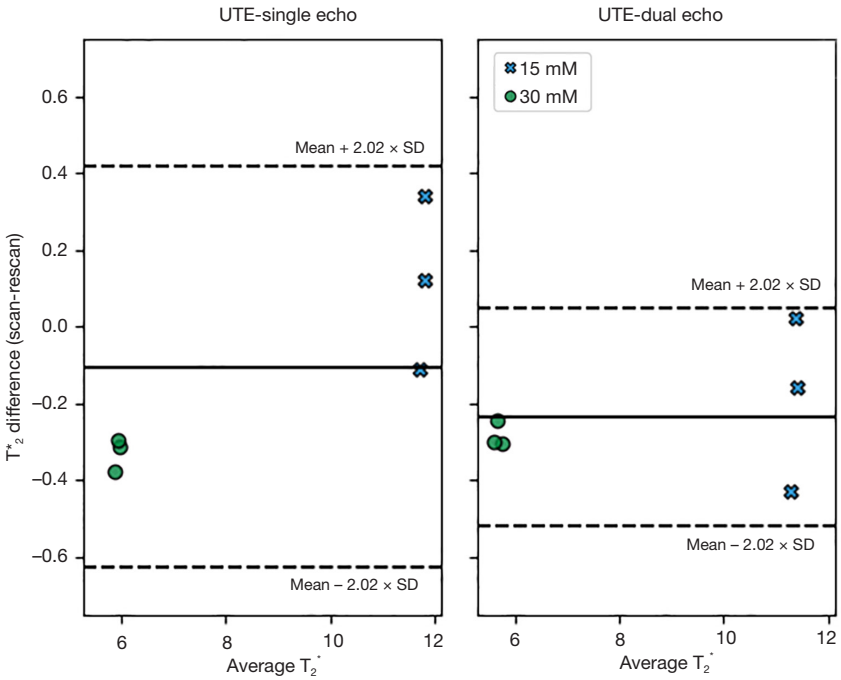

Figure 3 Bland-Altman plots showing the difference *vs.* average T_2* relaxation time between scan and rescan images from phantom images acquired using single and dual echo UTE sequences for different phantom ROIs. The solid line shows the mean difference between scan and rescan T_2* relaxation times, and the dashed lines show the limits of agreement. UTE, ultra-short echo time; SD, standard deviation; ROI, region of interest.

of the T_2* relaxation time is repeatable between scanning sessions, although there was some variation between phantoms. The percent difference values for 30 mM phantom were higher than the 15 mM Gd values across sequences. One potential reason for the observed differences could be shorter T_2* relaxation time and rapidly decaying signal in the 30 mM phantom (*Figure 2*) causing later echoes to be more affected by noise and introducing variation in T_2* quantifications. The phantom images from the GRE sequence generally had higher percent difference for mean T_2* relaxation time compared to the UTE sequence for both phantoms (*Table 4*), which may be because the GRE sequence has a relatively long TE for the first echo, leading to lower SNR in the first TE image compared with the UTE sequence (19). In general, both UTE and GRE T_2* repeatability are sensitive to image SNR, and efforts should be made to increase SNR and minimize the noise-induced variations to provide better quantitative reproducibility.

Fat suppression and the number of radial spokes used after fat suppression had little effect on UTE-T_2* relaxation times in phantoms and tissue, as indicated by the low CVs between results with and without fat suppression, which are further supported by the high ICC value (0.99) indicating excellent agreement (*Table 5*). It was observed that the *ex vivo* tissue's UTE-T_2* relaxation times with fat suppression were slightly longer compared to those without fat suppression (*Table 5*). One potential reason for this difference could be that fat suppression has little effect on the homogeneous phantom with T_2* >5 ms (for both phantoms), but the ultra-short T_2* (<5 ms) components in the tissues may be affected by fat suppression. Short T_2* tissues have a broader spectral bandwidth which can overlap with the frequency band of the fat saturation pulse, and signals in the ultra-short T_2* component tissues could therefore also be partially saturated, leading to a lower signal intensity at UTE. A relatively long duration fat suppression pulse with narrower bandwidth could reduce signal attenuation of short T_2* tissues but would potentially decrease the quality of fat saturation (21).

In vivo UTE-T_2* relaxation times of ligament, tendon, and menisci obtained from our sequence were generally consistent with the literature where similar sequences were

© Quantitative Imaging in Medicine and Surgery. All rights reserved.

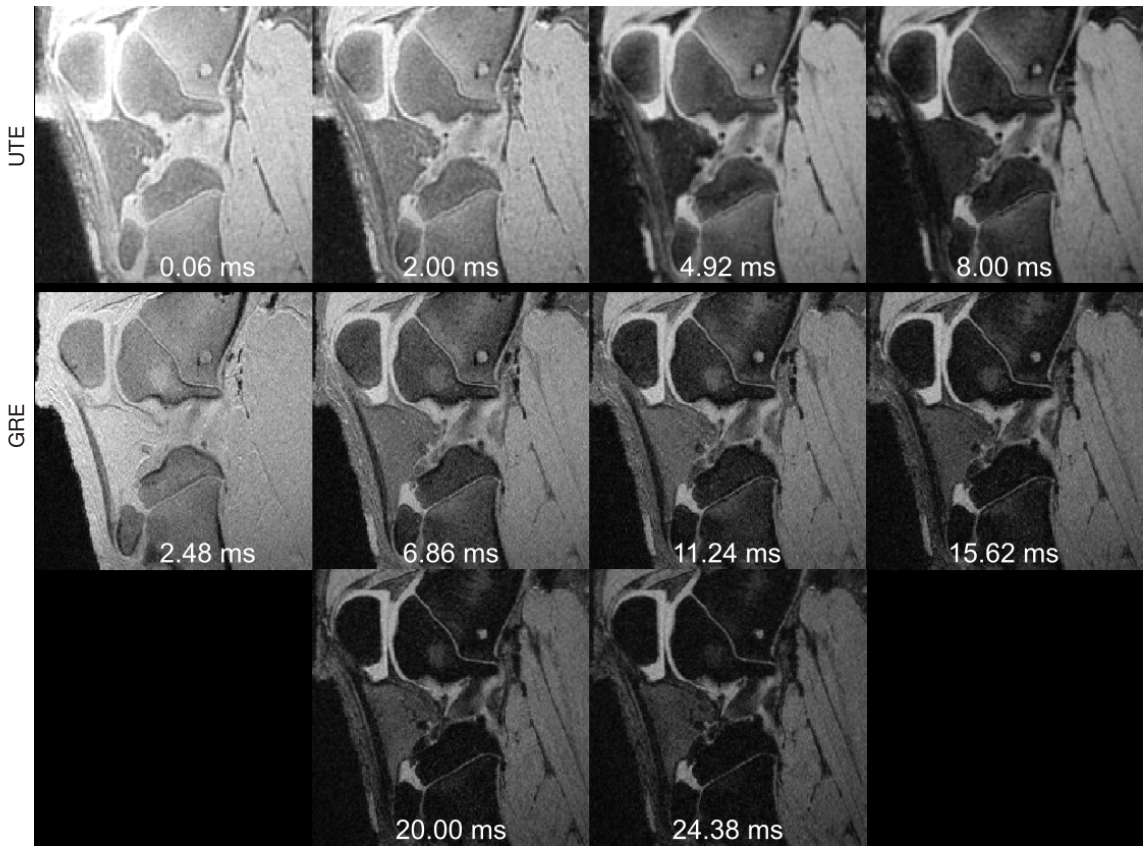

Figure 4 Representative slices from the *ex-vivo* pig knee UTE and GRE images with 20 radial spokes after fat suppression preparation showing the four and six echoes, respectively. UTE, ultra-short echo time; GRE, gradient echo.

Table 5 The GRE-T_2* and dual-echo UTE-T_2* relaxation times for the *ex-vivo* specimen and phantoms, and the UTE-T_2* CV and ICC for Gd phantoms and each tissue in the *ex-vivo* specimen without fat suppression and with different numbers of radial spokes after fat suppression

Sequence	15 mM Gd	30 mM Gd	ACL	PCL	PT	MEN
GRE-T_2* (ms)			16.14±6.58	21.54±8.49	9.00±2.69	11.65±4.92
UTE-T_2* (ms)						
None	11.31±0.20	5.59±0.013	9.80±3.15	12.69±2.76	4.18±0.56	8.12±1.90
Spokes # 5	11.31±0.19	5.76±0.029	10.94±3.80	14.11±2.98	4.51±0.95	8.30±2.06
Spokes # 10	11.22±0.18	5.70±0.032	10.69±3.59	13.91±3.06	4.33±0.91	8.27±1.96
Spokes # 15	11.16±0.20	5.68±0.033	10.64±3.63	13.67±2.88	4.23±0.85	8.28±1.99
Spokes # 20	11.14±0.18	5.65±0.031	10.44±3.73	13.61±3.14	4.20±0.85	8.19±2.05
Overall CV (UTE-T_2*)	0.72%	1.10%	4.10%	4.01%	3.17%	0.91%
Fat suppressed CV (UTE-T_2*)	0.68%	0.82%	1.93%	1.66%	3.24%	0.58%
Overall ICC (UTE-T_2*)	0.993 (0.975–0.999)					

Overall CV and ICC values were calculated across all of the images. The fat suppressed CV values were calculated across only the fat suppressed images. Data are presented as mean ± standard deviation, CV, and the ICC with 95% confidence intervals. GRE, gradient echo; UTE, ultra-short echo time; CV, coefficient of variation; ICC, intraclass correlation coefficient; Gd, gadolinium; ACL, anterior cruciate ligament; PCL, posterior cruciate ligament; PT, patellar tendon; MEN, meniscus.

© Quantitative Imaging in Medicine and Surgery. All rights reserved.

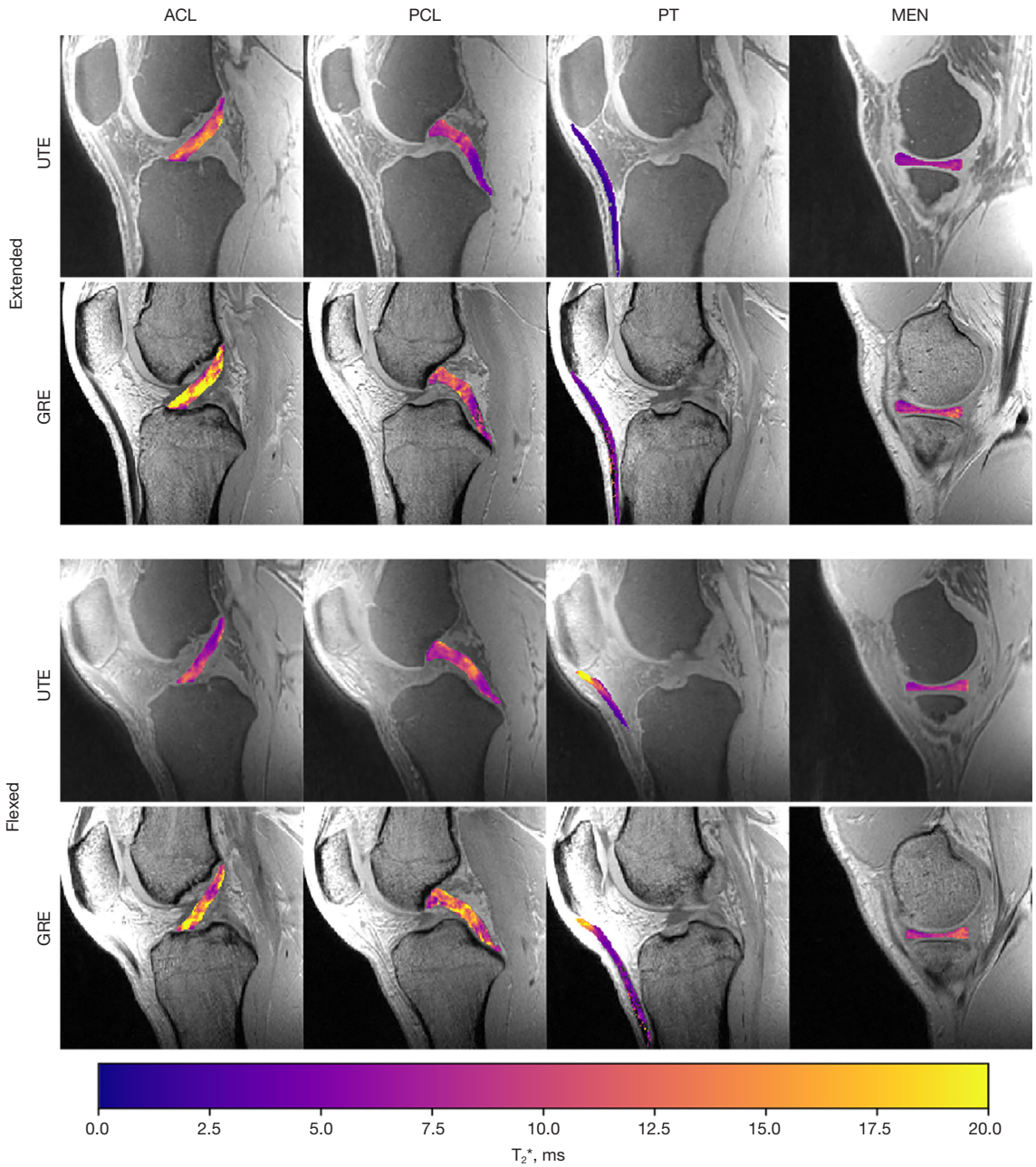

Figure 5 Representative slices of the first echo of one subject's extended and flexed UTE and GRE images with an overlay of the T_2* relaxation time map for each tissue. UTE, ultra-short echo time; GRE, gradient echo; ACL, anterior cruciate ligament; PCL, posterior cruciate ligament; PT, patellar tendon; MEN, meniscus.

implemented. The present ACL UTE-T_2* relaxation time was 11.9 ms, which is similar to that reported from *in vitro* (11.3 ms) (18), but shorter than has been reported *in vivo* (~16 ms) (15,17). This current study's meniscus UTE-T_2* relaxation time (7.4 ms) was near the lower range of values previously reported for the anterior and posterior meniscus regions (8.5–11.7 ms) (6,16,17). The difference between our results and those previously reported could stem from regional differences within the menisci, where the current study evaluated the meniscal body (*Figure 5*) rather than

© Quantitative Imaging in Medicine and Surgery. All rights reserved.

Table 6 *In vivo* UTE- and GRE-T_2* relaxation time for each tissue in the extended and flexed knee position for all subjects, the ICC between extended and flexed positions for the UTE and GRE images, and the % Diff of T2* values between the UTE and GRE sequences

Sequence	ACL	PCL	PT	MEN
UTE-T_2* (ms)				
Extended knee	11.91±1.64	7.52±0.68	2.87±0.66	7.44±0.30
Flexed knee	8.48±1.10	9.03±0.69	6.06±2.69	7.64±0.63
ICC	0.511 (0.089–0.775)			
GRE-T_2* (ms)				
Extended knee	20.09±2.17	10.82±1.13	7.22±1.78	8.87±0.39
Flexed knee	15.04±2.12	12.04±0.88	6.17±1.01	8.88±0.77
ICC	0.769 (0.501–0.902)			
UTE *vs.* GRE (% Diff)				
Extended knee	51.45±6.05	35.84±6.76	83.05±31.15	17.46±6.27
Flexed knee	55.73±3.92	28.55±2.78	25.70±18.98	14.91±3.72

Data are presented as the mean ± standard deviation and the ICC with the 95% confidence interval. UTE, ultra-short echo time; GRE, gradient echo; % Diff, percent difference; ICC, intraclass correlation coefficient; ACL, anterior cruciate ligament; PCL, posterior cruciate ligament; PT, patellar tendon; MEN, meniscus.

Table 7 The RMSD, % Diff, and ICC between T_2* relaxation times calculated using extended and flexed knee images and scan and rescan images

Sequence	ACL	PCL	PT	MEN
UTE-T_2*				
Extend/flex (n=5)				
RMSD (ms)	3.93	1.87	4.31	0.76
% Diff	33.17±17.66	18.28±12.96	63.23±38.65	8.26±5.33
Scan/rescan (n=4)				
RMSD (ms)	0.24	0.34	0.39	0.54
% Diff	1.89±1.65	3.26±2.30	7.29±7.09	6.67±3.05
ICC	0.985 (0.958–0.995)			
GRE-T_2*				
Extend/flex (n=5)				
RMSD (ms)	5.66	1.64	2.22	0.46
% Diff	28.86±14.41	12.84±6.04	22.47±18.39	4.87±2.17
Scan/rescan (n=3)				
RMSD (ms)	0.22	0.26	0.32	0.48
% Diff	1.05±0.88	1.98±1.46	4.91±2.38	4.80±2.14
ICC	0.997 (0.988–0.999)			

Data are presented as the mean ± standard deviation and the ICC with the 95% confidence interval. RMSD, root mean square deviation; % Diff, percent difference; ICC, intraclass correlation coefficient; ACL, anterior cruciate ligament; PCL, posterior cruciate ligament; PT, patellar tendon; MEN, meniscus; UTE, ultra-short echo time; GRE, gradient echo.

© Quantitative Imaging in Medicine and Surgery. All rights reserved.

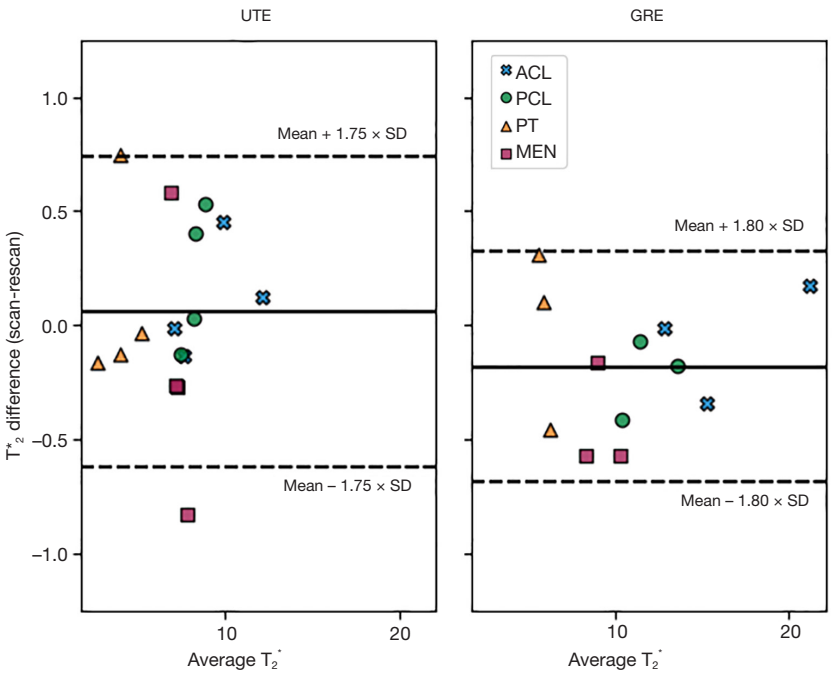

Figure 6 Bland-Altman plots showing the difference *vs.* average T_2* relaxation time between scan and rescan images from in-vivo images acquired using the dual-echo UTE and multi-echo GRE sequences for different tissue ROIs. The solid line shows the mean difference between scan and rescan T_2* relaxation time values, and the dashed lines show the limits of agreement. UTE, ultra-short echo time; GRE, gradient echo; ACL, anterior cruciate ligament; PCL, posterior cruciate ligament; PT, patellar tendon; MEN, meniscus; SD, standard deviation; ROIs, regions of interest.

the anterior or posterior meniscal horns. The reported PT UTE-T_2* relaxation time (2.9 ms) fell within the range that has been reported for healthy subjects (2.0–5.7 ms) (14,17), and the current study's PCL UTE-T_2* relaxation time (7.5 ms) was similar to previously reported (8.8 ms) for *in-vivo* subjects (17), and shorter than has been reported for *ex-vivo* specimens (11.1 ms) (34).

T_2* relaxation times quantified from the phantoms showed excellent agreement between UTE and GRE sequences (ICC =0.99, *Table 4*), however, the values quantified from knee tissues showed poor agreement between sequences, with average percent differences ranging between 15–85% (*Table 6*). One potential reason for this difference could be that knee tissues are characterized by short and long T_2* components (35), and the UTE sequence detects short T_2* components which are not well captured by the conventional GRE sequence (36). The additional signal from the ultrashort echo could result in different T_2* relaxation time quantifications between UTE and GRE sequences. The phantoms may not show the same variation between sequences because their signal decay may be characterized by a single component, resulting in similar T_2* relaxation times between UTE and GRE sequences. Implementing bi-exponential fitting in both UTE- and GRE-derived images may resolve these *in vivo* sequence-specific differences and could be explored in future work. Additionally, the difference in T_2* relaxation time between the UTE and GRE sequences could be due to the *ex-vivo* and *in-vivo* UTE sequence parameters having a longest echo that is one third of the longest echo in the GRE sequence (*Table 1*). Adding longer echoes to the UTE sequence that are comparable to the GRE sequence would provide a more direct comparison, however it would also prohibitively increase the scan time.

The UTE and GRE sequences demonstrated repeatability *in vivo*, however, knee position introduced variability into T_2* relaxation time quantifications for the evaluated ligaments and tendon. Both sequences showed ICC values greater than 0.98 (*Table 7*) between *in vivo* scan-rescan images, demonstrating excellent agreement. The meniscus had a consistently low RMSD between T_2* values quantified from extended and flexed knee positions. Chu

© Quantitative Imaging in Medicine and Surgery. All rights reserved.

et al. (6) showed significant differences of 2.7 and 5.0 ms in meniscal UTE-T_2* relaxation time between uninjured controls and preoperative ACL tear patients with uninjured and injured menisci, respectively. This current study showed that the RMSD in meniscus UTE-T_2* relaxation for repeated scans and different knee positions was less than 1 ms (*Table* 7), which suggests that the evaluated UTE sequence would be sensitive enough to detect clinically relevant changes in meniscus T_2* relaxation times. The same group (15) also showed a significant 2 ms change in mean ACL graft UTE-T_2* relaxation time between 1 and 2 years post-operatively, which is less than this current study's reported RMSD of 4 ms between knee positions, but markedly greater than the RMSD of 0.24 ms reported between repeated scans (*Table* 7). The RMSD in ACL UTE-T_2* values between repeated scans and knee positions indicates that the applied UTE sequence can be sensitive enough to evaluate ACL graft maturation *in vivo*, however, the reproducibility of ACL UTE-T_2* quantifications is impacted by knee position reproducibility.

The sensitivity of T_2* relaxation time to knee position can originate from multiple sources. One explanation could be the magic angle effect, which causes increasing overestimation of T_2* relaxation time as the orientation of the tissue's organized collagen approaches 54° relative to the static B_0 field (22-24). The anatomic orientation of the ACL, PCL and PT may make these tissues more susceptible to the magic angle effect in the evaluated knee positions, resulting in variation of T_2* relaxation time quantification between extended and flexed positions. Conversely, the meniscus is likely less affected by the magic angle effect because of its anatomic orientation in the evaluated joint positions. Changes in ligament and tendon tensioning between knee positions could be another source of variation in mean T_2* values between knee positions, where T_2* relaxation time may change as ligament tensioning changes between extended and flexed positions (37-39).

There are several limitations for our study worth noting. First, the sample size for this study was small, and including additional subjects would enhance the robustness of our findings. Additionally, only two knee positions were considered when evaluating the effect that knee position has on T_2* relaxation time quantifications. The results show that UTE and GRE T_2* quantifications can change due to knee position, however, a more systematic approach with multiple knee positions would be needed to characterize the orientation dependence of T_2* relaxation time. A more systematic approach could also evaluate changes in joint rotations aside from flexion, such as varus and internal tibial rotation to account for potential coupled kinematics. As suggested earlier, the use of a mono-exponential fitting function to determine T_2* relaxation times could introduce bias to the tissue's UTE- and GRE-T_2* relaxation time calculations and implementing a bi-exponential fitting function as others have done (35,40) may reduce this sequence-specific bias. Further to this point, separating short and long T_2* components could provide additional sensitivity to detect clinically meaningful tissue remodeling processes and is of interest in future work developing these sequences.

Conclusions

In summary, we showed that the 3D radial UTE sequence can be used to repeatably quantify T_2* relaxation time for knee ligaments, tendons, and menisci. The meniscus showed little variation in UTE-T_2* values between evaluated knee positions, suggesting that the presented UTE sequence can yield reproducible T_2* quantifications. The scan-rescan repeatability of the ACL UTE-T_2* values indicates that the presented sequence may be used to detect clinically relevant changes in mean T_2* relaxation time, however, reproducibility of these values is impacted by knee position consistency between scans.

Acknowledgments

Funding: This study was partially supported by NIH/NIBIB U01EB023829 (PIs: Xiaoliang Zhang and Xiaojuan Li), NIH/NIAMS R00-AR069004 (PI: Jillian E. Beveridge), NIH T32AR007505 (Awardee: William Zaylor), and the Cleveland Clinic Musculoskeletal Research Center (001-IF102433, PI: Jillian E. Beveridge).

Footnote

Conflicts of Interest: All authors have completed the ICMJE uniform disclosure form (available at https://qims.amegroups.com/article/view/10.21037/qims-23-459/coif). Kecheng Liu is employed by Siemens Medical Solutions USA, Inc., Malvern. Xiaodong Zhong was an employee of Medical Solutions USA, Inc. in Los Angeles until June 30, 2023. Stefan Sommer is employed by Siemens Healthineers International AG, Switzerland. Jillian E. Beveridge and

© Quantitative Imaging in Medicine and Surgery. All rights reserved.

William Zaylor received partial salary support from NIH/NIAMS R00-AR069094, and William Zaylor also received salary support from NIH T32AR007505. Xiaojuan Li and Xiaoliang Zhang received partial salary support from the grant NIH/NIBIB U01EB023829, and the same grant partially supported the work presented in this study. The other authors have no conflicts of interest to declare.

Ethical Statement: The authors are accountable for all aspects of the work in ensuring that questions related to the accuracy or integrity of any part of the work are appropriately investigated and resolved. This study was conducted in accordance with the Declaration of Helsinki (as revised in 2013) and approved by the Institutional Review Board of the Cleveland Clinic, written informed consent was obtained from the participants prior to human subject experiments.

Open Access Statement: This is an Open Access article distributed in accordance with the Creative Commons Attribution-NonCommercial-NoDerivs 4.0 International License (CC BY-NC-ND 4.0), which permits the non-commercial replication and distribution of the article with the strict proviso that no changes or edits are made and the original work is properly cited (including links to both the formal publication through the relevant DOI and the license). See: https://creativecommons.org/licenses/by-nc-nd/4.0/.

References

1. Hasegawa A, Otsuki S, Pauli C, Miyaki S, Patil S, Steklov N, Kinoshita M, Koziol J, D'Lima DD, Lotz MK. Anterior cruciate ligament changes in the human knee joint in aging and osteoarthritis. Arthritis Rheum 2012;64:696-704.
2. Levy YD, Hasegawa A, Patil S, Koziol JA, Lotz MK, D'Lima DD. Histopathological changes in the human posterior cruciate ligament during aging and osteoarthritis: correlations with anterior cruciate ligament and cartilage changes. Ann Rheum Dis 2013;72:271-7.
3. Naoum S, Mitseas P, Koutserimpas C, Kotsapas M, Raptis K, Gantsos AS. Correlation of Cruciate Ligament Histological Findings with Coronal Plane Deformities and Characteristics of Patients Undergoing Total Knee Arthroplasty. Maedica (Bucur) 2022;17:323-8.
4. Thorpe CT, Screen HR. Tendon Structure and Composition. Adv Exp Med Biol 2016;920:3-10.
5. Benjamin M, Milz S, Bydder GM. Magnetic resonance imaging of entheses. Part 2. Clin Radiol 2008;63:704-11.
6. Chu CR, Williams AA, West RV, Qian Y, Fu FH, Do BH, Bruno S. Quantitative Magnetic Resonance Imaging UTE-T2* Mapping of Cartilage and Meniscus Healing After Anatomic Anterior Cruciate Ligament Reconstruction. Am J Sports Med 2014;42:1847-56.
7. Wang A, Pedoia V, Su F, Abramson E, Kretzschmar M, Nardo L, Link TM, McCulloch CE, Jin C, Ma CB, Li X. MR T1ρ and T2 of meniscus after acute anterior cruciate ligament injuries. Osteoarthritis Cartilage 2016;24:631-9.
8. Rauscher I, Stahl R, Cheng J, Li X, Huber MB, Luke A, Majumdar S, Link TM. Meniscal measurements of T1rho and T2 at MR imaging in healthy subjects and patients with osteoarthritis. Radiology 2008;249:591-600.
9. Baum T, Joseph GB, Karampinos DC, Jungmann PM, Link TM, Bauer JS. Cartilage and meniscal T2 relaxation time as non-invasive biomarker for knee osteoarthritis and cartilage repair procedures. Osteoarthritis Cartilage 2013;21:1474-84.
10. Su X, Zhang Y, Gao Q, Liang Z, Wan L, Zhang L, Tang G. Preliminary study on the assessment of early cartilage degeneration by quantitative ultrashort echo time magnetic resonance imaging in vivo. Quant Imaging Med Surg 2022;12:3803-12.
11. Amiel D, Frank C, Harwood F, Fronek J, Akeson W. Tendons and ligaments: a morphological and biochemical comparison. J Orthop Res 1984;1:257-65.
12. Robson MD, Gatehouse PD, Bydder M, Bydder GM. Magnetic resonance: an introduction to ultrashort TE (UTE) imaging. J Comput Assist Tomogr 2003;27:825-46.
13. Chang EY, Du J, Chung CB. UTE imaging in the musculoskeletal system. J Magn Reson Imaging 2015;41:870-83.
14. Kijowski R, Wilson JJ, Liu F. Bicomponent ultrashort echo time T2* analysis for assessment of patients with patellar tendinopathy. J Magn Reson Imaging 2017;46:1441-7.
15. Chu CR, Williams AA. Quantitative MRI UTE-T2* and T2* Show Progressive and Continued Graft Maturation Over 2 Years in Human Patients After Anterior Cruciate Ligament Reconstruction. Orthop J Sports Med 2019;7:2325967119863056.
16. Yi J, Lee YH, Song HT, Suh JS. Comparison of T2* mapping between regular echo time and ultrashort echo time with 3D cones at 3 tesla for knee meniscus. Medicine (Baltimore) 2018;97:e13443.
17. Wu M, Zhao W, Wan L, Kakos L, Li L, Jerban S, Jang H, Chang EY, Du J, Ma YJ. Quantitative three-dimensional

© Quantitative Imaging in Medicine and Surgery. All rights reserved.

ultrashort echo time cones imaging of the knee joint with motion correction. NMR Biomed 2020;33:e4214.
18. Jerban S, Hananouchi T, Ma Y, Namiranian B, Dorthe EW, Wong JH, Shojaeiadib N, Wu M, Du J, D'Lima D, Chung CB, Chang EY. Correlation between the elastic modulus of anterior cruciate ligament (ACL) and quantitative ultrashort echo time (UTE) magnetic resonance imaging. J Orthop Res 2022;40:2330-9.
19. Williams A, Qian Y, Chu CR. UTE-T2* mapping of human articular cartilage in vivo: a repeatability assessment. Osteoarthritis Cartilage 2011;19:84-8.
20. Agergaard AS, Malmgaard-Clausen NM, Svensson RB, Nybing JD, Boesen M, Kjaer M, Magnusson SP, Hansen P. UTE T2* mapping of tendinopathic patellar tendons: an MRI reproducibility study. Acta Radiol 2021;62:215-24.
21. Carl M, Nazaran A, Bydder GM, Du J. Effects of fat saturation on short T2 quantification. Magn Reson Imaging 2017;43:6-9.
22. Shao H, Pauli C, Li S, Ma Y, Tadros AS, Kavanaugh A, Chang EY, Tang G, Du J. Magic angle effect plays a major role in both T1rho and T2 relaxation in articular cartilage. Osteoarthritis Cartilage 2017;25:2022-30.
23. Du J, Pak BC, Znamirowski R, Statum S, Takahashi A, Chung CB, Bydder GM. Magic angle effect in magnetic resonance imaging of the Achilles tendon and enthesis. Magn Reson Imaging 2009;27:557-64.
24. Wu M, Ma Y, Wan L, Jerban S, Jang H, Chang EY, Du J. Magic angle effect on adiabatic T(1ρ) imaging of the Achilles tendon using 3D ultrashort echo time cones trajectory. NMR Biomed 2020;33:e4322.
25. Beveridge JE, Machan JT, Walsh EG, Kiapour AM, Karamchedu NP, Chin KE, Proffen BL, Sieker JT, Murray MM, Fleming BC. Magnetic resonance measurements of tissue quantity and quality using T(2) * relaxometry predict temporal changes in the biomechanical properties of the healing ACL. J Orthop Res 2018;36:1701-9.
26. Flannery SW, Murray MM, Badger GJ, Ecklund K; Kramer DE, Fleming BC, Kiapour AM. Early MRI-based quantitative outcomes are associated with a positive functional performance trajectory from 6 to 24 months post-ACL surgery. Knee Surg Sports Traumatol Arthrosc 2023;31:1690-8.
27. Li X, Benjamin Ma C, Link TM, Castillo DD, Blumenkrantz G, Lozano J, Carballido-Gamio J, Ries M, Majumdar S. In vivo T(1rho) and T(2) mapping of articular cartilage in osteoarthritis of the knee using 3 T MRI. Osteoarthritis Cartilage 2007;15:789-97.
28. Peters JR, Zaylor W, Chokhandre SK, Klonowski EM, Erdemir A, Beveridge JE, Li X. An Automated Approach to Define Femoral and Tibial Coordinate Systems with Limited Diaphysis Length. In: Orthopaedic Research Society Annual Meeting. Dallas Texas; 2023.
29. Grood ES, Suntay WJ. A joint coordinate system for the clinical description of three-dimensional motions: application to the knee. J Biomech Eng 1983;105:136-44.
30. Gamer M, Lemon J, Fellows I, Singh P. irr: Various Coefficients of Interrater Reliability and Agreement [Internet]. 2019 [cited 2022 May 5]. Available from: https://CRAN.R-project.org/package=irr
31. Koo TK, Li MY. A Guideline of Selecting and Reporting Intraclass Correlation Coefficients for Reliability Research. J Chiropr Med 2016;15:155-63.
32. Zhu D, Wu W, Yu W, Hong G, Fang Y, Li S, Ma Y. Ultrashort echo time magnetization transfer imaging of knee cartilage and meniscus after long-distance running. Eur Radiol 2023;33:4842-54.
33. Chen Y, Li L, Le N, Chang EY, Huang W, Ma YJ. On the fat saturation effect in quantitative ultrashort TE MR imaging. Magn Reson Med 2022;87:2388-97.
34. Wilms LM, Radke KL, Latz D, Thiel TA, Frenken M, Kamp B, Filler TJ, Nagel AM, Müller-Lutz A, Abrar DB, Nebelung S. UTE-T2* versus conventional T2* mapping to assess posterior cruciate ligament ultrastructure and integrity-an in-situ study. Quant Imaging Med Surg 2022;12:4190-201.
35. Liu J, Nazaran A, Ma Y, Chen H, Zhu Y, Du J, Li S, Zhou Q, Zhao Y. Single- and Bicomponent Analyses of T2∗ Relaxation in Knee Tendon and Ligament by Using 3D Ultrashort Echo Time Cones (UTE Cones) Magnetic Resonance Imaging. Biomed Res Int 2019;2019:8597423.
36. Williams A, Qian Y, Bear D, Chu CR. Assessing degeneration of human articular cartilage with ultra-short echo time (UTE) T2* mapping. Osteoarthritis Cartilage 2010;18:539-46.
37. Csapo R, Juras V, Heinzle B, Trattnig S, Fink C. Compositional MRI of the anterior cruciate ligament of professional alpine ski racers: preliminary report on seasonal changes and load sensitivity. Eur Radiol Exp 2020;4:64.
38. Jerban S, Nazaran A, Cheng X, Carl M, Szeverenyi N, Du J, Chang EY. Ultrashort echo time T2(*) values decrease in tendons with application of static tensile loads. J Biomech 2017;61:160-7.

© Quantitative Imaging in Medicine and Surgery. All rights reserved.

39. Wilms LM, Radke KL, Abrar DB, Latz D, Schock J, Frenken M, Windolf J, Antoch G, Filler TJ, Nebelung S. Micro- and Macroscale Assessment of Posterior Cruciate Ligament Functionality Based on Advanced MRI Techniques. Diagnostics (Basel) 2021;11:1790.
40. Chang EY, Du J, Statum S, Pauli C, Chung CB. Quantitative bi-component T2* analysis of histologically normal Achilles tendons. Muscles Ligaments Tendons J 2015;5:58-62.

Cite this article as: Wu Z, Zaylor W, Sommer S, Xie D, Zhong X, Liu K, Kim J, Beveridge JE, Zhang X, Li X. Assessment of ultrashort echo time (UTE) T_2* mapping at 3T for the whole knee: repeatability, the effects of fat suppression, and knee position. Quant Imaging Med Surg 2023;13(12):7893-7909. doi: 10.21037/qims-23-459

© Quantitative Imaging in Medicine and Surgery. All rights reserved.